Lasing threshold control in two-dimensional photonic crystals with gain

Sotiris Droulias,[1,*] Chris Fietz,[2] Peng Zhang,[2] Thomas Koschny,[2] and Costas M. Soukoulis[1,2]

[1]*Institute of Electronic Structure and Laser, FORTH, 71110 Heraklion, Crete, Greece*
[2]*Ames Laboratory and Department of Physics and Astronomy, Iowa State University, Ames, Iowa 50011, USA*
[*]*sdroulias@iesl.forth.gr*

Abstract: We demonstrate how the lasing threshold of a two dimensional photonic crystal containing a four-level gain medium is modified, as a result of the interplay between the group velocity and the modal reflectivity at the interface between the cavity and the exterior. Depending on their relative strength and the optical density of states, we show how the lasing threshold may be dramatically altered inside a band or, most importantly, close to the band edge. The idea is realized via self-consistent calculations based on a finite-difference time-domain method. The simulations are in good agreement with theoretical predictions.

References and links

1. H. Kogelnik and C. V. Shank, "Stimulated emission in a periodic structure," Appl. Phys. Lett. **18**(4), 152–154 (1971).
   H. Kogelnik and C. V. Shank, "Coupled-wave theory of distributed feedback lasers," J. Appl. Phys. **43**(5), 2327–2335 (1972).
2. J. P. Dowling, M. Scalora, M. J. Bloemer, and C. M. Bowden, "The photonic band edge laser: A new approach to gain enhancement," J. Appl. Phys. **75**(4), 1896–1899 (1994).
3. M. D. Tocci, M. Scalora, M. J. Bloemer, J. P. Dowling, and C. M. Bowden, "Measurement of spontaneous-emission enhancement near the one-dimensional photonic band edge of semiconductor heterostructures," Phys. Rev. A **53**(4), 2799–2803 (1996).
4. M. Meier, A. Mekis, A. Dodabalapur, A. Timko, R. Slusher, J. Joannopoulos, and O. Nalamasu, "Laser action from two-dimensional distributed feedback in photonic crystals," Appl. Phys. Lett. **74**(1), 7 (1999).
5. M. Imada, S. Noda, A. Chutinan, T. Tokuda, M. Murata, and G. Sasaki, "Coherent two-dimensional lasing action in surface-emitting laser with triangular-lattice photonic crystal structure," Appl. Phys. Lett. **75**(3), 316 (1999).
6. S. Riechel, C. Kallinger, U. Lemmer, J. Feldmann, A. Gombert, V. Wittwer, and U. Scherf, "A nearly diffraction limited surface emitting conjugated polymer laser utilizing a two-dimensional photonic band structure," Appl. Phys. Lett. **77**(15), 2310–2312 (2000).
7. H.-Y. Ryu, S.-H. Kwon, Y.-J. Lee, Y.-H. Lee, and J.-S. Kim, "Very-low-threshold photonic band-edge lasers from free-standing triangular photonic crystal slabs," Appl. Phys. Lett. **80**(19), 3476–3478 (2002).
8. S.-H. Kwon, H.-Y. Ryu, G.-H. Kim, Y.-H. Lee, and S.-B. Kim, "Photonic bandedge lasers in two-dimensional square-lattice photonic crystal slabs," Appl. Phys. Lett. **83**(19), 3870–3872 (2003).
9. X. Wu, A. Yamilov, X. Liu, S. Li, V. P. Dravid, R. P. H. Chang, and H. Cao, "Ultraviolet photonic crystal laser," Appl. Phys. Lett. **85**(17), 3657–3659 (2004).
10. F. Raineri, G. Vecchi, A. M. Yacomotti, C. Seassal, P. Viktorovitch, R. Raj, and A. Levenson, "Doubly resonant photonic crystal for efficient laser operation: Pumping and lasing at low group velocity photonic modes," Appl. Phys. Lett. **86**(1), 011116 (2005).
11. C. Karnutsch, M. Stroisch, M. Punke, U. Lemmer, J. Wang, and T. Weimann, "Laser diode-pumped organic semiconductor lasers utilizing two-dimensional photonic crystal resonators," Phot. Tech. Lett. **19**(10), 741–743 (2007).
12. D. Luo, X. W. Sun, H. T. Dai, Y. J. Liu, H. Z. Yang, and W. Ji, "Two-directional lasing from a dye-doped two-dimensional hexagonal photonic crystal made of holographic polymer-dispersed liquid crystals," Appl. Phys. Lett. **95**(15), 151115 (2009).
13. W. Cao, A. Muñoz, P. Palffy-Muhoray, and B. Taheri, "Lasing in a three-dimensional photonic crystal of the liquid crystal blue phase II," Nat. Mater. **1**(2), 111–113 (2002).
14. B. D'Urso, O. Painter, J. Brien, T. Tombrello, A. Yariv, and A. Scherer, "Modal reflectivity in finite-depth two-dimensional photonic crystal microcavities," J. Opt. Soc. Am. B **15**, 1155–1159 (1998).

15. K. Sakoda, "Enhanced light amplification due to group-velocity anomaly peculiar to two- and three-dimensional photonic crystals," Opt. Express **4**(5), 167–176 (1999).
16. S. Nojima, "Optical-gain enhancement in two-dimensional active photonic crystals," J. Appl. Phys. **90**(2), 545–551 (2001).
17. L. Florescu, K. Busch, and S. John, "Semiclassical theory of lasing in photonic crystals," J. Opt. Soc. Am. B **19**(9), 2215–2223 (2002).
18. H.-Y. Ryu, M. Notomi, and Y.-H. Lee, "Finite-difference time-domain investigation of band-edge resonant modes in finite-size two-dimensional photonic crystal slab," Phys. Rev. B **68**(4), 045209 (2003).
19. N. Susa, "Threshold gain and gain-enhancement due to distributed-feedback in two-dimensional photonic-crystal lasers," J. Appl. Phys. **89**(2), 815–823 (2001).
20. P. Bermel, E. Lidorikis, Y. Fink, and J. D. Joannopoulos, "Active materials embedded in photonic crystals and coupled to electromagnetic radiation," Phys. Rev. B **73**(16), 165125 (2006).
21. S. V. Zhukovsky and D. N. Chigrin, "Numerical modelling of lasing in microstructures," Phys. Status Solidi **244**(10), 3515–3527 (2007).
22. X. Hu, J. Cao, M. Li, Z. Ye, M. Miyawaki, and K.-M. Ho, "Modeling of three-dimensional photonic crystal lasers in a frequency domain: A scattering matrix solution," Phys. Rev. B **77**(20), 205104 (2008).
23. A. Fang, T. Koschny, and C. M. Soukoulis, "Lasing in metamaterial nanostructures," J. Opt. **12**(2), 024013 (2010).
24. C. Fietz and C. M. Soukoulis, "Finite element simulation of microphotonic lasing system," Opt. Express **20**(10), 11548–11560 (2012).
25. C. Fietz, "Absorbing boundary condition for Bloch-Floquet eigenmodes," J. Opt. Soc. Am. B **30**(10), 2615–2620 (2013).
26. Y. Pinhasi, A. Yalalom, and G. A. Pinhasi, "Propagation analysis of ultrashort pulses in resonant dielectric media," J. Opt. Soc. Am. B **26**(12), 2404–2413 (2009).

1. Introduction

Lasing action can be achieved with three ingredients: a gain medium, a pump source and a feedback mechanism. The most intuitive approach to the feedback mechanism has traditionally been a set of mirrors placed outside the gain medium volume, allowing for the photon recurrence. This approach has served well up to now for bulk laser systems, but as technology has shifted to the nanoscale, the need for miniaturized feedback schemes has become crucial. Over the decades alternative ideas have been proposed for the realization of high Q cavities with small sizes. The Bragg mirror realized the necessary end reflectors in the microscale and the distributed Bragg reflector (DBR) incorporated the feedback mechanism within the gain medium (DFB - Distributed Feedback lasers) [1].

In 1994 Dowling et. al. proposed a one-dimensional Photonic Crystal (PC) operating at the band edge [2], instead of the center of the band gap like the previous DFB lasers. Simply put, near the band edge the group velocity approaches zero and the photons undergoing multiple reflections in the lattice experience longer interaction with the gain material, thus resulting in an enhanced effective gain. This approach allowed for the realization of a laser system with only a few layers of alternating material and a large index variation, as opposed to the DFB laser of small refractive index modulation that required thousands of periods [3]. Since then, the concept of the band edge laser has been generalized to PC structures of higher dimensions. Experimentally, the idea has been demonstrated in 2D [4–12] and 3D configurations as well [13], and several theoretical works have examined various pertinent lasing aspects [14–24].

In all previous works, the lasing features (e.g. emitted power, lasing threshold) have been analyzed mainly in terms of the cavity Q factor [7,8,14,17,18], which incorporates all effects that lead to radiation loss, thus obscuring the separate role of each constituent. Among them the group velocity has been investigated [15–18], but its connection with the modal reflectivity at the interface of the cavity with the exterior is either missing or considered only via effective parameters that do not reveal their separate contribution to the Q factor [14,17].

In this work we investigate the lasing threshold in microstructured systems containing a four level gain medium and show how it can be modified as a result of the interplay between the group velocity and interface reflectivity of the lasing mode. To this end, we establish a simple theoretical model that decomposes the contributions of these features to the Q factor. In order to demonstrate them in realistic structures we choose a 2D PC of a finite amount of layers as testbed. Our simulations show that operation near the band edge can lead to strong reduction of the lasing threshold with respect to a uniform gain slab of the same dimensions,

in spite of the lower gain density, even for as few as 10 layers. Moreover, with a slight structural modification, the PC is surprisingly demonstrated to exhibit lower lasing threshold at steeper band edges. Our self-consistent finite-difference time-domain (FDTD) calculations are explained in a straightforward manner by the theoretical model, which may also predict other counter-intuitive behaviors, such as lower lasing threshold inside a band, rather than the band edge.

2. The two-dimensional photonic crystal system and the self-consistent model

The 2D PC consists of air columns inside a dielectric background, in a square lattice configuration. This makes the structure easy in manufacturing and mechanically robust, as compared to the complementary system of dielectric columns embedded in air. For simplicity the air holes are chosen to have square cross section with side w. The system is assumed to be infinite along the y, z directions and finite along the x direction with a total length of $L = n \times a$, where n is the number of layers and a the lattice constant. The permittivity of the dielectric background is chosen to be $\varepsilon_r = 11.7$, as high refractive index contrasts between the two materials of the PC (the 2nd material being the air) enhance the band flattening near the Brillouin zone edges and lead to lower group velocities [16]. Moreover, the unit cell properties are set to $a = 840nm$ and $w = 540nm$, which give a gain density of $V_{gain}/V_{cavity} \cong 59\%$, i.e. 41% lower than that of a uniform slab. This choice ensures that the 1st band gap for the TE polarization is full and prominent, while maintaining as much gain material as possible (smaller air holes that allow for more gain material reduce the band gap). The system for the case of $n = 10$ layers is shown in Fig. 1, where the respective homogeneous gain slab of same length is also depicted. The band structure for the TE polarization of the 2D PC is also shown. The shaded zone denotes the full band gap and the red line marks the edge of the ΓX direction, along which the system is studied.
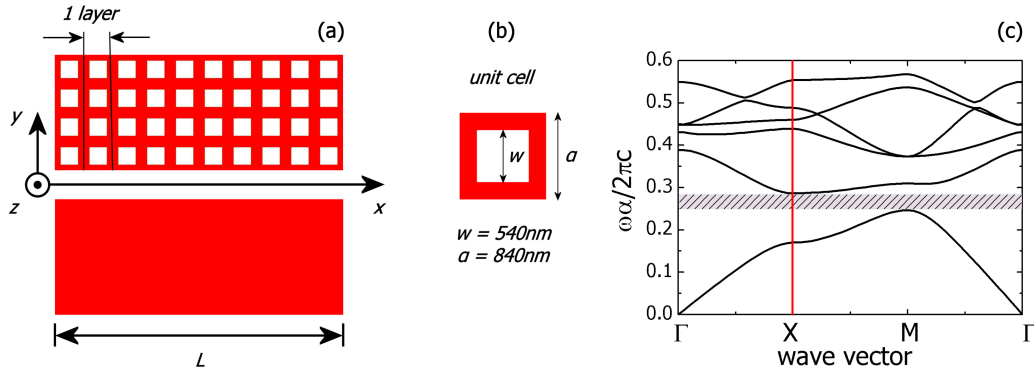
Fig. 1. (a) Schematic of the 2D PC consisting of 10 layers (top) and the respective slab of uniform gain and same length (bottom). The red areas denote the host dielectric of $\varepsilon_r = 11.7$, which is homogeneously embedded with the four level gain material. Both systems are infinite in the yz plane and confined in the x direction, along which the emitted wave propagates. (b) Unit cell of the 2D PC (c) Calculated band structure for the TE polarization of the infinite version of the 2D PC. The shaded zone denotes the full bandgap.

The gain material is homogeneously embedded in the dielectric host medium and is modeled as a simple four level quantum system, as described in our previous works (for details, see [23,24]). It is assumed to have a Lorentzian response which is homogeneously broadened and centered at ω_a (emission frequency) with linewidth Γ_a. The gain material is characterized by the lifetimes $\tau_{10} = 10^{-13} s$, $\tau_{21} = 10^{-10} s$, $\tau_{32} = 10^{-12} s$ and $\tau_{30} = 10^{-11} s$. The coupling constant is $\sigma_a = 10^{-4} \, C^2/kg$ and the linewidth of the corresponding transition is

$\Gamma_a = 2\pi \times 2 \times 10^{12} \, Hz$. In our FDTD simulations the total electron density is considered to be $N_0(t=0) = N_0(t) + N_1(t) + N_2(t) + N_3(t) = 5 \times 10^{23} \, m^{-3}$. The initial condition is that all electrons are in the ground state and all electric, magnetic and polarization fields are zero. The electrons are homogeneously pumped from N_0 to N_3 with a constant pump rate R_p and the system of the Maxwell equations coupled with the atomic rate equations is self-consistently solved. This procedure is repeated for several pump rates and the emitted optical power, P_{out}, is calculated for each input R_p. For high pump rates, far above the lasing threshold, P_{out} varies nonlinearly in terms of R_p, but as the threshold is approached the variation becomes linear. This validates the linear extrapolation of the calculated data close to the lasing threshold, the determination of which might otherwise demand prohibitively large computational times. In all FDTD calculations the discrete time and space steps are set to $t = 50 \times 10^{-18} s$ and $x = 30 \times 10^{-9} m$, respectively. The emission frequency ω_a is chosen for each case separately, as a free design parameter.

3. Theoretical model for the Q factor

Let us consider a cavity of length L, formed by a finite amount of layers of the photonic crystal, in which a pulse with carrier frequency ω_0 and spectral width $\Delta\omega$ recirculates, as depicted in Fig. 2. Assuming $\Delta\omega \ll \omega_0$, the pulse evolves spatially as a single Bloch mode. Let the pulse be written as a product of the optical carrier $\exp(i\omega_0 t)$ and an envelope function, so that $E_0(t) = e^{i\omega_0 t} \int E_{env}(\Omega) e^{i\Omega t} d\Omega$, where $\Omega = \omega - \omega_0$ and $E_{env}(\Omega)$ is the Fourier spectrum of the baseband envelope. At each round trip each spectral component accumulates $2kL + Arg(r_{21}) + Arg(r_{23})$ phase shift and decreases in amplitude by a factor of $|r_{21}||r_{23}|(1-p)$, where k is the wavenumber of the Bloch mode, r_{21}, r_{23} the complex modal reflectivities at each interface and p the fractional internal power loss parameter due to possible material absorption. After m round-trips the pulse is written as $E_m(t) = e^{i\omega_0 t} \int E_{env}(\Omega) e^{-i(\beta - ia)m2L} e^{i\Omega t} d\Omega$, where $\beta = k + (2L)^{-1}(Arg(r_{21}) + Arg(r_{23}))$ and $a = -(2L)^{-1} \ln(|r_{21}||r_{23}|(1-p)) \geq 0$, that constitute the complex propagation constant.
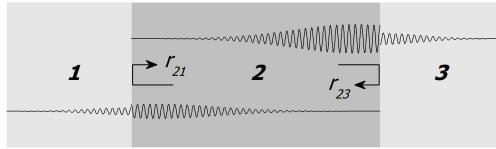
Fig. 2. Schematic of the recirculating pulse approach. The pulse travels with group velocity v_g inside the cavity and bounces back and forth at the boundary with each semi-infinite exterior space. r_{ij} is the reflectivity of the electric field travelling in area i that bounces at the interface with area j.

Expansion of $\beta - ia$ around ω_0 yields $\beta - ia = \beta_0 - ia_0 + \Omega(\beta_1 - ia_1) + \dfrac{\Omega^2}{2}(\beta_2 - ia_2) + \cdots$, with $\beta_n \triangleq d^n\beta/d\omega^n\big|_{\omega=\omega_0}$ and $a_n \triangleq d^n a/d\omega^n\big|_{\omega=\omega_0}$ ($n = 0,1,2\ldots$). Assuming a high Q cavity, the term $k_1 \triangleq dk/d\omega\big|_{\omega=\omega_0}$ –located in β_1– dominates over the higher order terms, especially close to the band edge where $k_1 \to \infty$, and the expansion can be truncated to 1st order. Thus, after a few calculations, $E_m(t) = e^{-a_0 m2L} e^{i(\omega_0 t - \beta_0 m2L)} E_0(t - m\tau_{rt})$, where $\tau_{rt} = k_1 2L$ is the round-trip time.

The respective intensity can be written as $I_m(t) = \exp(-m\tau_{rt}/\tau_c)I_0(t)$ with $\tau_c = -k_1 L/\ln(|r_{21}||r_{23}|(1-p))$ and $I_0(t) = |E_0(t - m\tau_{rt})|^2$, expressing the decay in small bursts every τ_{rt} with rate $1/\tau_c$. If $\tau_c \gg \tau_{rt}$ the radiation bursts become smooth function of time and the intensity is simply $I_m(t) = \exp(-t/\tau_c)I_0(t)$. The energy stored in the cavity U_s, follows the same temporal decay and, in the absence of power supply, the power dissipated is simply $P_d = -\partial U_s/\partial t = (1/\tau_c)U_s$. Hence, $Q \triangleq \omega \times (U_s/P_d) = \omega\tau_c$ or

$$Q = -\frac{\omega L}{v_g \ln(|r_{21}||r_{23}|(1-p))} \tag{1}$$

where $v_g = 1/k_1$ is the group velocity. This expression summarizes the fact that, if the boundaries become more reflective or if the energy can be made bounce back and forth at a slower pace, the rate at which energy escapes from the cavity can be reduced. In essence, less pumping is needed for the same emitted power to be achieved and the lasing threshold, which is the minimum pump rate at which the gain compensates for optical losses at the boundaries and for possible material absorption at each round-trip, is accordingly reduced. In general, since the group velocity is a property of the infinite system, separate modification of the reflectivity, which is a boundary effect, can offer flexibility in the tuning of the Q factor. Last, for pulses beyond the quasi-monochromatic limit and/or highly lossy/dispersive cavities, Eq. (1) will be modified, as higher order terms in the expansion need to be retained [26], thus deviating from this simple form which is adequate for the high Q systems we are interested in.

4. Lasing in dielectric slab with gain

Let us first consider the simple homogeneous slab as cavity. In this case the Q factor may cast a purely analytical form. The reflectivity at the interface between two semi-infinite homogeneous media labeled i, j is given by $r_{ij} = (z_j - z_i)/(z_j + z_i)$, where $z_i = \sqrt{\mu_i/\varepsilon_i}$ and $z_j = \sqrt{\mu_j/\varepsilon_j}$ are the relative impedances of the two media. In our case the slab of relative permittivity ε_r is surrounded by air and, as such, $\mu_1 = \mu_2 = \mu_3 = 1$, $\varepsilon_1 = \varepsilon_3 = 1$ and $\varepsilon_2 = \varepsilon_r$. Assuming negligible material dispersion, the group velocity equals the phase velocity, i.e. $v_g = c/\sqrt{\varepsilon_r}$, where c is the light velocity in vacuum. Ignoring internal losses, Eq. (1) now yields $Q = \omega L \times (\sqrt{\varepsilon_r}/2c) \ln((\sqrt{\varepsilon_r}+1)/(\sqrt{\varepsilon_r}-1))^{-1}$ (2). This simple linear relation between Q and ωL states that – within the range of its validity – less pumping is needed for the same output power either if the operating frequency is increased or if the system is elongated. Both situations translate into the possibility for lower lasing thresholds.

Typically, when the system is pumped, if the pump rate is sufficient for population inversion the system will start to lase at a frequency, which is determined by the gain material emission frequency ω_a and the Fabry-Perot resonances $\omega_{FP} = q\pi c/L\sqrt{\varepsilon_r}$ ($q = 1, 2, 3...$) of the cavity – ω_{FP} referring to the unpumped system. When lasing starts, the overall permittivity, which is nonlinearly dependent on the pump, is slightly changed within a frequency range of Γ_a, around the frequency ω_a. This change alone, when countable, is sufficient to invalidate the conclusions drawn by the simple form of Eq. (2). Moreover, if ω_a does not coincide with a certain ω_{FP}, then the cavity resonance will shift, rendering lasing more power demanding. Fortunately, as the lasing threshold is approached, the overall permittivity approaches the host material permittivity and the resonances converge to those of the unpumped system: the lasing system lases approximately at ω_a. Given the experimental feasibility, tuning $\omega_a = \omega_{FP}$ should thus be a good starting point.

To illustrate these conclusions, let us examine the performance of three gain slabs of length $L_1 = 10a$, $L_2 = 20a$ and $L_3 = 30a$. In the simulations we pump the system, let it radiate and, after the lasing amplitude is stabilized, we measure the output EM field at a certain distance from the cavity and extract the output lasing power for this specific pump rate. The output lasing power versus the input pump rate for the examined cases is presented in Fig. 3.
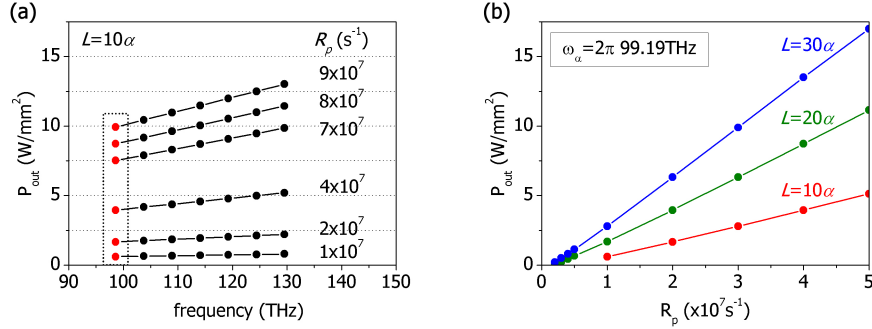
Fig. 3. (a) Lasing power of a gain slab with $L = 10a$ at successive Fabry-Perot resonances and for different pump rates. Each set of connected points is an iso-pump line. The red points inside the dotted box are reproduced partly in (b) on the red line. (b) Lasing power at $\omega = \omega_{FP} = \omega_a = 2\pi\ 99.19$THz for different pump rates. Three gain slabs are analyzed, all with the same material properties, but with different lengths, namely $L_1 = 10a$ (red), $L_2 = 20a$ (green) and $L_3 = 30a$ (blue), where $a = 840nm$. The lasing threshold is reduced with increasing slab length, as expected.

First, the slab of length $L_1 = 10a$ is examined at successive Fabry-Perot resonances, as shown in Fig. 3(a), where, for each case, the emission peak of the gain material is set to coincide with the respective ω_{FP}. Due to the negligible change of the Q factor among these operating frequencies, the lasing threshold changes only slightly. On the other hand it is clear that as the operating frequency increases less pumping is needed in order to achieve the same output power. In Fig. 3(b) the three systems are compared at a common ω_{FP}. This is set to $99.19THz$, which is close to the operation frequency of the PC above the 1st bandgap, to be examined later. In essence, we assume that the slabs are all embedded with the same gain material, which has an emission peak exactly at $99.19THz$. It is evident that the lasing threshold is reduced with increasing slab length, as expected. The Q factor in these configurations is rather low due to the poor reflectivity ($|r_{21}| = |r_{23}| \cong 0.55$) and the lasing threshold is reduced within the same order of magnitude, i.e. no severe lowering is achieved, unless the slab is extremely elongated. Both v_g and $|r|$ are constant, except perhaps a negligible frequency dispersion induced by $\varepsilon_r = \varepsilon_r(\omega)$, and their contributions to Q do not exhibit anything dramatic as the operating frequency changes.

5. Lasing in dielectric 2D photonic crystal with gain

In the case of the finite 2DPC system, Eq. (1) is calculated semi-analytically. The group velocity is a property of the infinite system and is derived directly from the dispersion curve (Fig. 4(a)) by differentiation along the ΓX direction, as $v_g = \partial\omega/\partial k$ (black line in Fig. 4(b)). The reflectivity of the Bloch modes inside the semi-infinite PC is calculated with a finite element (FEM) simulation (grey lines in Fig. 4(b)) [25]. Due to the symmetry of the unit cell the cavity is terminated in the same way at both ends and consequently $|r_{21}| = |r_{23}| \triangleq |r|$. Internal losses are assumed absent and all data are inserted into Eq. (1) to give a Q factor envelope, as depicted with a white line in Fig. 4(c). This envelope serves as the locus of the Q points for any system of arbitrary length, regardless of the exact frequency position of the resonances. This fact is verified with another set of FEM eigenfrequency simulations, where the complex frequency ω of the field (simulation eigenvalue) expresses the radiative losses.

The results of the simulations are interpreted as $Q = \mathrm{Re}(\omega)/2\mathrm{Im}(\omega)$, consistently with the definition in section 3, i.e. $\mathrm{Im}(\omega) = 1/2\tau_c$. They are depicted in Figs. 4(d)–4(f) for three (unpumped) systems of length $L_1 = 10a$, $L_2 = 20a$ and $L_3 = 30a$, respectively. These results, normalized to each system's number of layers $n = L/a$ and mapped on the same scale, coincide with the semi-analytical Q/n envelope (Fig. 4(c)).
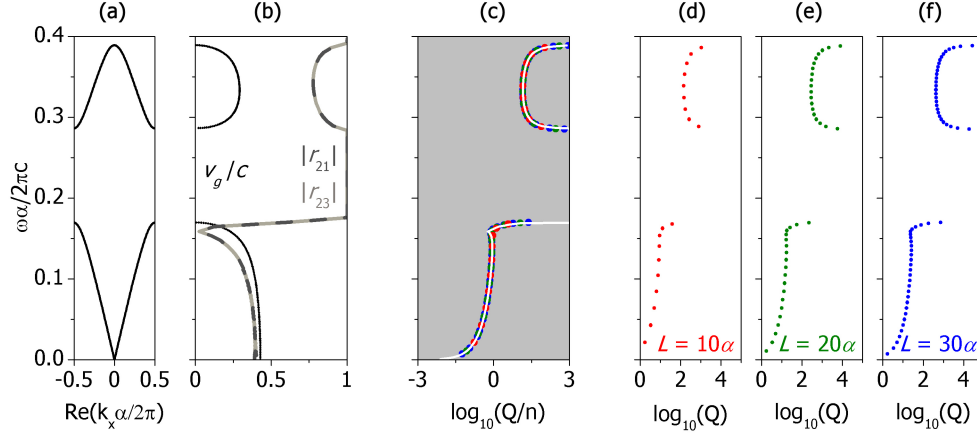
Fig. 4. Calculations for the passive photonic crystal pictured in Fig. 1. (a) Dispersion curve along the ΓX direction of the infinite system. (b) Normalized group velocity v_g/c and interface reflectivities $|r_{21}| = |r_{23}|$ of the Bloch modes. (c) Q envelope (white line) from semi-analytical Eq. (1) normalized with number of layers $n = L/a$ and overlapped with simulated Q/n for the three finite systems of length $L_1 = 10a$ (red), $L_2 = 20a$ (green) and $L_3 = 30a$ (blue). For clarity these are shown unnormalized separately in (d), (e) and (f).

A simple inspection of Fig. 4 shows that, as in the homogeneous slab, Q is improved in longer systems, simply because the optical power traveling at v_g stays longer in the system before losing a fraction of $1-|r|^2$ at the interface. The picture, though, is far richer. A longer PC now offers a higher number of optical density of states (DOS), allowing for a resonance to be situated closer to a band edge, where Q can grow dramatically. In essence, as a band edge is approached, $v_g \to 0$ and $|r| \to 1$. These conditions boost Q, although not arbitrarily high, since in a finite system the band edge cannot be approached arbitrarily close. The contribution from both v_g and $|r|$ is depicted in Fig. 4(b) and verifies the fact that for points of the same v_g, Q is higher at those with the higher $|r|$. A cross section at e.g. $v_g/c = 0.25$ finds one point in band 1 and two points in band 2 of clearly higher $|r|$, which are characterized by higher Q. Inversely, for points of the same $|r|$, Q is indeed higher at those with lower v_g.

To correlate the lasing threshold with these conclusions we performed FDTD simulations on the three systems of length $L_1 = 10a$, $L_2 = 20a$ and $L_3 = 30a$. The results are separated into two sets and summarized in Fig. 5. One set of simulations regards the examination of the lasing threshold in a certain system (we chose $L_1 = 10a$) as the frequency is swept throughout the resonances (Figs. 5(a) and 5(b)). A second set regards comparison among different systems, at frequencies close to the band edges of the 1st band gap (Figs. 5(c) and 5(d)), namely at ~60THz (below the gap) and ~100THz (above). As mentioned, for the finite systems these frequencies are better approached with increasing cavity length. As with the slab, the gain material emission frequency ω_a was tuned for each case exactly at the examined cavity resonance.
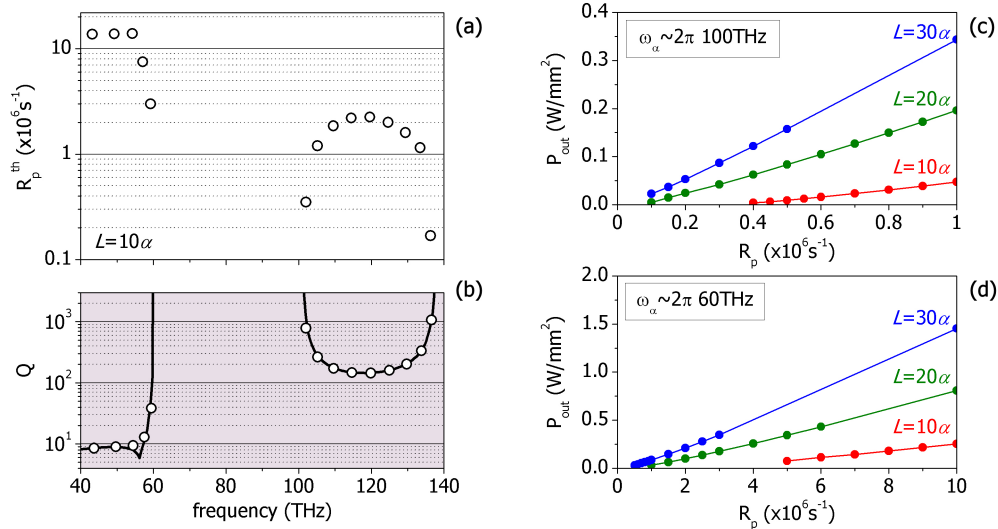
Fig. 5. (a) Lasing threshold for the system of length $L_1 = 10a$. (b) Simulated Q factor (open circles) overlapped with the semi-analytical Q factor envelope (solid line). (c) Lasing power for different pump rates above and (d) below the 1st bandgap, for the three 2DPC's of length $L_1 = 10a$ (red), $L_2 = 20a$ (green) and $L_3 = 30a$ (blue). Notice that the thresholds in (c) are 1 order of magnitude lower than in (d). In all cases the lasing threshold varies consistently with Q.

In Fig. 5(b) the simulated Q factor for the system of length $L_1 = 10a$ already presented in Fig. 4 is shown again for easier comparison with the lasing threshold depicted in Fig. 5(a). It is evident that the lasing threshold varies consistently with the Q factor. The same observation holds for the 2nd set of simulations among the three systems. The lasing threshold reduces as the cavity is elongated, both above the band gap (Fig. 5(c)) and below (Fig. 5(d)). Moreover, it drops one order of magnitude when going from lower to upper band edge. The PC performs better than the slab, despite the lower gain density, except at some frequencies deep in the 1st band. This is not a surprise, because the PC reflectivity in the 1st band is lower than that of the slab (except close to the band edge) and, also, below ~50THz the group velocity in the PC becomes greater than in the slab. On the other hand a PC is more likely to operate at the band edges, where the dramatic increase of the DOS offers a unique design versatility. Since the exact emission frequency ω_a of the gain material may have a countable frequency tolerance due to experimental limitations during manufacturing, a system with dense resonances ω_R increases the probability of ω_a, ω_R matching and consequently of lower lasing threshold.

6. Discussion

The group velocity is a property of the infinite system and cannot be modified simply by truncating the 2DPC at a certain finite length. On the other hand, the reflectivity is a boundary effect and can be tuned either by changing the termination plane within the unit cell or by extending the interface with another system, homogeneous or not. To illustrate this we investigated two systems which bear all the properties of the examined 2DPC system, but the air hole is shifted along the x-axis, thus maintaining the periodicity. In the 1st system the hole has been shifted 420nm (half unit cell) and in the 2nd system 150nm, touching the edge of the unit cell, as shown in the insets of Figs. 6(b) and 6(c). Both systems are $L = 10a$ long and their schematics together with the simulations are shown in Fig. 6.
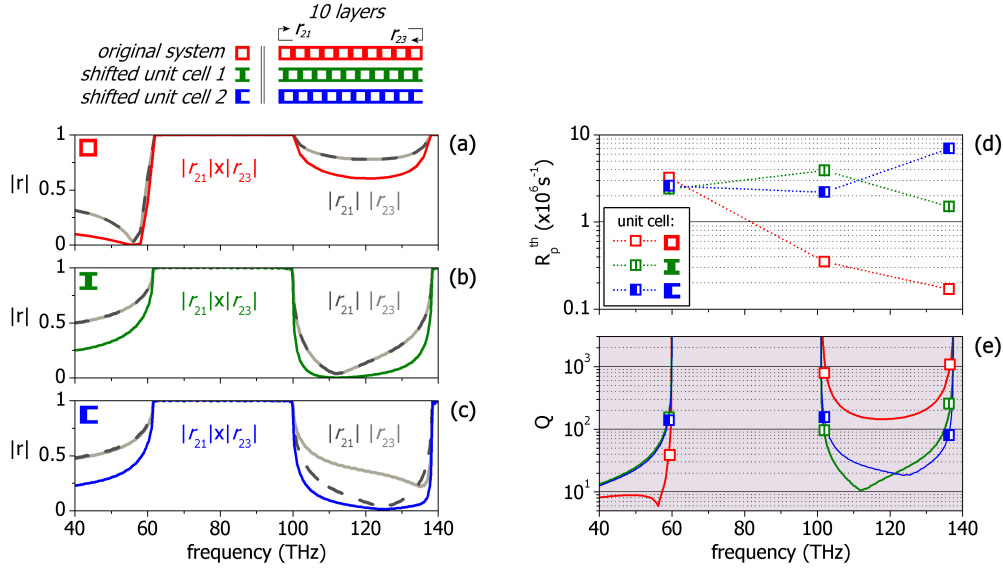
Fig. 6. Calculated reflectivities $|r_{21}|,|r_{23}|$ and their product that determines Q for (a) the original system of $n = 10$ layers and (b), (c) its modified versions (see inset for unit cell). (d) Calculated lasing threshold and (e) Q factor at the edges of the 1st and 2nd band in log scale. In (e) the semi-analytical Q envelope as calculated with the data from (a), (b) and (c) is also shown as solid line. The dotted lines in (d) are shown for easier comparison among calculated points and do not imply a piece-wise monotonic change in the pump rate threshold. Also, the color code denotes the unit cell structure and should not be confused with the previous figures.

The 1st system (Fig. 6(b)) preserves both periodicity and symmetry and hence $|r_{21}| = |r_{23}|$. The 2nd system (Fig. 6(c)) preserves the periodicity, but breaks the symmetry when finite in length and $|r_{21}| \neq |r_{23}|$. In both cases though, their product which determines Q improves in the 1st band and drops significantly in the 2nd band (compare with Fig. 6(a) which corresponds to the original system). This has the expected impact on the Q envelope and is reflected accordingly in the lasing threshold, which now drops below the band gap (~60THz) but becomes higher at the bottom and top of the 2nd band (~100THz and ~136THz respectively), as shown in Fig. 6(d). The great increase of the threshold in band #2 is a result of the great change in Q (by a factor of 5~12), as compared to the change in the 1st band, where Q is enhanced by a factor of 3~4. The 1st system, in particular, manifests a huge dip towards the bottom of the 2nd band. As a result, the lasing threshold at those frequencies increases to levels even higher than those of the 1st band. On the other hand, for the 2nd system the dip is situated towards the top of the band, where the lasing threshold is pushed to a level higher than that of the bottom of the same band. These results express a more general remark: a dip in the reflectivity may affect the overall performance of a system severely, even if the group velocity is very low, as for example close to a band edge. Hence, lower lasing thresholds at sharper band edges or even inside some band should not be a surprise, especially in narrow bands with sparse resonances. Of course, longer systems with enhanced DOS will gradually eliminate this paradox, as more resonances will shift closer to the band edges. The results from Figs. 5(a) and 5(b) regarding the lasing threshold and Q factor at the edges of the 1st and 2nd band are reproduced in Figs. 6(d) and 6(e) respectively, for easier comparison.

7. Conclusion

In this work we have studied the lasing threshold of a two dimensional photonic crystal containing a four-level gain medium in terms of the Q factor and the optical density of states. The contributions from the group velocity and the interface reflectivity to the Q factor,

although related, were decomposed and it was shown that, depending on their relative strength, the lasing threshold may dramatically be altered. Within this context we demonstrated that the lasing threshold of a 2DPC operating at the band edge can, in principle, be lower than that of the same system inside some band or of other homogeneous media of the same dimensions but of higher gain densities. Nevertheless, it was shown that the picture may be counter-intuitively changed and even reversed, especially for systems of low DOS. The calculations were based on a finite-difference time-domain method and were in good agreement with predictions, based on a simple theoretical model.

Acknowledgments